ARTHRITIS & RHEUMATISM
Vol. 58, No. 7, July 2008, pp 2065–2074
DOI 10.1002/art.23548

Biomechanics of Cartilage Articulation

Effects of Lubrication and Degeneration on Shear Deformation

Benjamin L. Wong,[1] Won C. Bae,[1] June Chun,[1] Kenneth R. Gratz,[1] Martin Lotz,[2] and Robert L. Sah[1]

Objective. **To characterize cartilage shear strain during articulation, and the effects of lubrication and degeneration.**

Methods. **Human osteochondral cores from lateral femoral condyles, characterized as normal or mildly degenerated based on surface structure, were selected. Under video microscopy, pairs of osteochondral blocks from each core were apposed, compressed 15%, and subjected to relative lateral motion with synovial fluid (SF) or phosphate buffered saline (PBS) as lubricant. When cartilage surfaces began to slide steadily, shear strain (E_{xz}) and modulus (G) overall in the full tissue thickness and also as a function of depth from the surface were determined.**

Results. **In normal tissue with SF as lubricant, E_{xz} was highest (0.056) near the articular surface and diminished monotonically with depth, with an overall average E_{xz} of 0.028. In degenerated cartilage with SF as lubricant, E_{xz} near the surface (0.28) was 5-fold that of normal cartilage and localized there, with an overall E_{xz} of 0.041. With PBS as lubricant, E_{xz} values near the articular surface were ~50% higher than those observed with SF, and overall E_{xz} was 0.045 and 0.062 in normal and degenerated tissue, respectively. Near the articular surface, G was lower with degeneration (0.06 MPa, versus 0.18 MPa in normal cartilage). In both normal and degenerated cartilage, G increased with tissue depth to 3–4 MPa, with an overall G of 0.26–0.32 MPa.**

Conclusion. **During articulation, peak cartilage shear is highest near the articular surface and decreases markedly with depth. With degeneration and diminished lubrication, the markedly increased cartilage shear near the articular surface may contribute to progressive cartilage deterioration and osteoarthritis.**

The tissue-scale mechanics of articular cartilage during the compressive and shear loading of joints with normal movement have not been fully characterized. After repeated knee bending (1) and running (2), articular cartilage is compressed by ~5–20% of its overall thickness. Within the cartilage tissue of dynamically compressed osteochondral blocks (3), the magnitude of compressive strain is highest near the articular surface and minimal in deeper regions, a pattern consistent with the depth-varying compressive modulus of cartilage (4). Despite extensive knowledge of cartilage compressive behavior, the overall and depth-varying shear deformation of cartilage during joint movement remains to be elucidated. Theoretical models of articulating joints can be used to predict local cartilage deformation (5,6), but are highly dependent on assumptions about boundary conditions at articulating surfaces (e.g., frictionless or adherent) and depth-varying mechanical properties (5). Detailed experimental characterization of apposing cartilage samples sliding relative to one another would further the understanding of cartilage mechanics during joint movement by elucidating the actual boundary condition at the articulating cartilage surface as well as the deformation and properties of cartilage in shear.

Lubrication of articulating cartilage by synovial fluid (SF) facilitates low friction in the boundary mode

Supported by the National Science Foundation and the NIH. Mr. Wong's work was supported in part by the San Diego Fellowship. Dr. Sah's work was supported by the Howard Hughes Medical Institute through the Professors Program Grant to the University of California, San Diego.

[1]Benjamin L. Wong, MS, Won C. Bae, PhD, June Chun, BS, Kenneth R. Gratz, MS, Robert L. Sah, MD, ScD: University of California, San Diego, La Jolla, California; [2]Martin Lotz, MD: Scripps Research Institute, La Jolla, California.

Mr. Wong and Dr. Bae contributed equally to this work.

Address correspondence and reprint requests to Robert L. Sah, MD, ScD, Department of Bioengineering, Mail Code 0412, University of California, San Diego, 9500 Gilman Drive, La Jolla, CA 92093-0412. E-mail: rsah@ucsd.edu.

Submitted for publication September 20, 2007; accepted in revised form March 18, 2008.

and may therefore affect the shear deformation of cartilage. When articulating cartilage is tested in a configuration that reveals boundary lubrication effects, SF and lubricant molecules in SF are shown to reduce articular surface interaction, as indicated by decreased friction (7,8). The replacement of SF lubricant with phosphate buffered saline (PBS) results in an elevation of boundary-mode friction (7). The dependence of local and overall shear deformation on SF may be important for maintenance of cartilage health, since acute injury or inflammatory arthritis results in reduced lubricating function of SF, and this may be involved in postinjury cartilage degeneration (9).

Cartilage degeneration may also affect the way in which the tissue deforms during joint movement. As cartilage undergoes degeneration, for example with aging (10), articular surfaces become fibrillated and roughened (11). Concomitantly, cartilage mechanical properties deteriorate under compressive, tensile, and shear loading (12), i.e., cartilage deformation and strain magnitude increase in response to a particular amplitude of applied load. Such mechanical deformation of cartilage affects chondrocyte metabolism, with moderate levels of dynamic compressive and shear strain stimulating matrix synthesis, but excessive levels inhibiting matrix synthesis (13). Thus, determination of the deformation and strain of articulating cartilage, with both normal and degenerated surfaces, would provide insight into the local mechanical cues that regulate chondrocyte behavior and the consequences of degenerative changes on such cues.

One experimental approach used to elucidate the local strain deformation and strain of cartilage is to track displacement of fiducial markers using a video microscopy system. Previous studies have focused on cartilage deformation and strain when samples were subjected to compression in the absence of applied shear (4,14,15). The depth-dependent compressive behavior of cartilage found in these microscale studies was consistent with findings in macroscopic tissue explants investigated by magnetic resonance imaging (3), and provided a resolution sufficient to resolve small magnitudes of strain (~1%). Thus, microscale analysis may also provide insight into cartilage shear deformation, both locally and overall. For studying cartilage shear deformation during joint movement (Figure 1A), a pair of osteochondral blocks (Figure 1B) can be compressed in apposition (Figure 1C) and subjected to lateral shearing motion (Figure 1D). Such a configuration can be controlled to mimic the biomechanical behavior of articulating cartilage at one scale (full-thickness tissue) and allow elucidation of cartilage deformation at a finer scale (regions of tissue measurements). Combined measurements of strain and stress allow determination of local and overall biomechanical properties such as shear modulus.

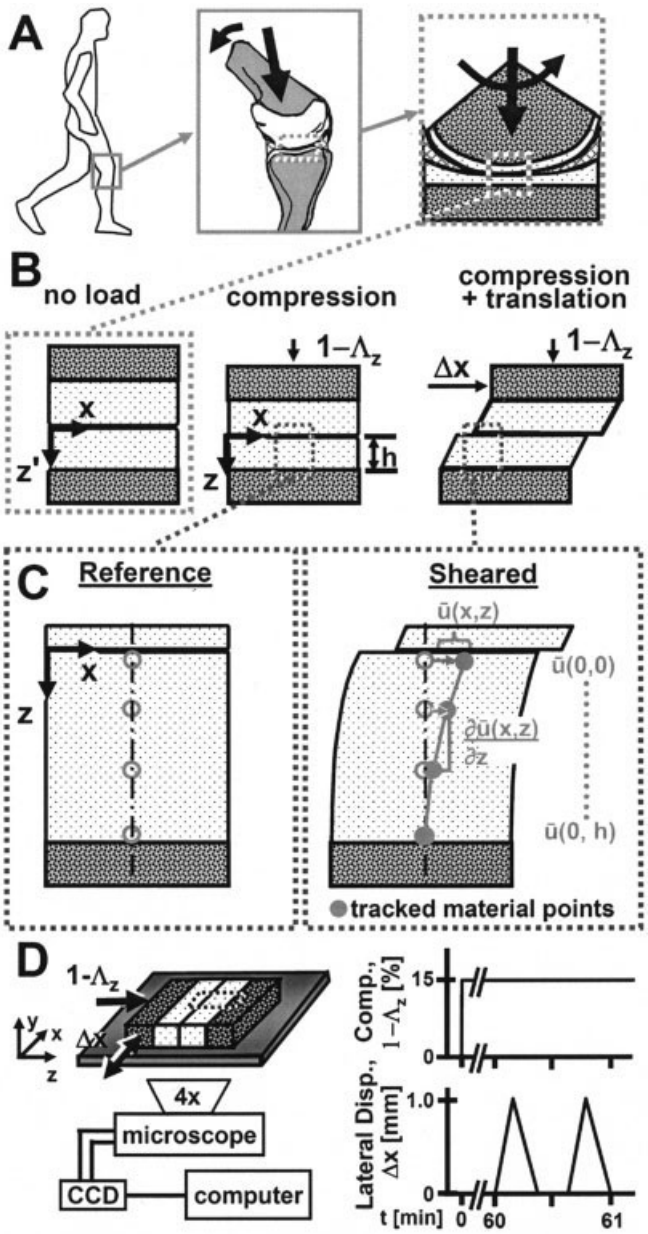

Figure 1. **A** and **B,** Schematic representation of knee joint movements at multiple scales (**A**), and deformation of cartilage under no load, compression (Comp.), and compression plus shear loading (**B**). **C,** Material points in compressed cartilage before and during shear loading used to determine ū(x,z) (depth-dependent displacement [Disp.] vectors), which were then used to assess intratissue deformation. **D,** Schematic representation of experimental setup and loading protocol for microscale shear testing.

Table 1. Age of the donors, and thickness and Mankin-Shapiro scores of the cartilage samples*

	Normal (n = 3)	Mildly degenerated (n = 3)
Age, years	48 ± 1.7	78 ± 9.2
Thickness, mm	1.86 ± 0.12	2.08 ± 0.15
Mankin-Shapiro score	1.89 ± 0.29	9.11 ± 1.24

* Values are the mean ± SEM.

The hypothesis of the present study was that during joint articulation, the shear deformation of cartilage is affected by both lubrication and degeneration. To test this, we implemented a cartilage-on-cartilage sliding test to microscopically observe and analyze cartilage deformation during compression and shear. With this system, we assessed the effects of lubrication (by SF versus PBS) and degeneration (normal versus mildly degenerated) on overall and depth-varying shear strain, and determined the overall and depth-varying shear modulus of normal and mildly degenerated cartilage.

MATERIALS AND METHODS

Sample isolation. Osteochondral cores (each with a diameter of 10 mm) were isolated from the anterior lateral femoral condyle of a single knee block from each of 6 fresh human cadaveric tissue donors (Table 1). Cores were chosen for this study based on the gross appearance of the articular surface, i.e., normal (n = 3) or mildly degenerated (n = 3). The surface was considered normal if the modified Outerbridge grade (16) was 1, and mildly degenerated if the grade was 3. Normal specimens were from donors ages 41–60 years at the time of death, and degenerated specimens were from donors age >60 years (Figures 2A and B). The cores were immersed in PBS containing proteinase inhibitors (PIs) and stored at −80°C until use.

Experimental design. On the day of testing, each core was thawed and prepared. The core was scored vertically in the cartilage using a razor blade and cut through the bone using a low-speed saw with a 0.3-mm–thick diamond-edge blade (Isomet; Buehler, Lake Bluff, IL) to yield an osteochondral fragment for histopathologic analysis and 2 approximately rectangular blocks for biomechanical testing. Each of the 2 blocks had a cartilage surface area of ~3 × 8 mm^2 and a total thickness of ~7 mm.

Histopathologic analysis. Histopathologic analysis was performed to assess and confirm the state of degeneration. Samples were fixed in 4% paraformaldehyde in PBS (pH 7.0) for 24 hours, decalcified with 18% disodium EDTA in PBS for 7 days, and sectioned to 7 μm using a cryostat. Some sections were stained with Alcian blue to localize sulfated glycosaminoglycans (GAGs), as previously described (17), and other sections were stained with hematoxylin and eosin to highlight cellular detail (18). Staining of samples resulted in a gradation of intensity (Figures 2C and D), reflecting the variation in GAG concentration with depth; thus, the staining method was sufficient to delineate GAG variation, such as loss due to pathology, and allow qualitative scoring. Transmitted light micrographs of the stained sections were obtained, and histologic features (19) analyzed using the Mankin-Shapiro semiquantitative scale (20). Briefly, the histopathologic characteristics assessed included structural integrity (surface irregularity and vertical and horizontal clefts), cellularity (cloning and hypocellularity), and GAG loss. A relatively high score represented more degenerated cartilage. Grades from 3 independent observers were averaged for each sample. Interobserver errors (SD) for normal and degenerated samples were reasonably small (average 1.0 and 2.1, respectively).

Biomechanical testing. Samples were first tested by microscale shear testing as described below, with PBS plus PI as the lubricant. Then, samples were allowed to reswell for ~4 hours at 4°C.

Next, samples were tested again by microscale shear

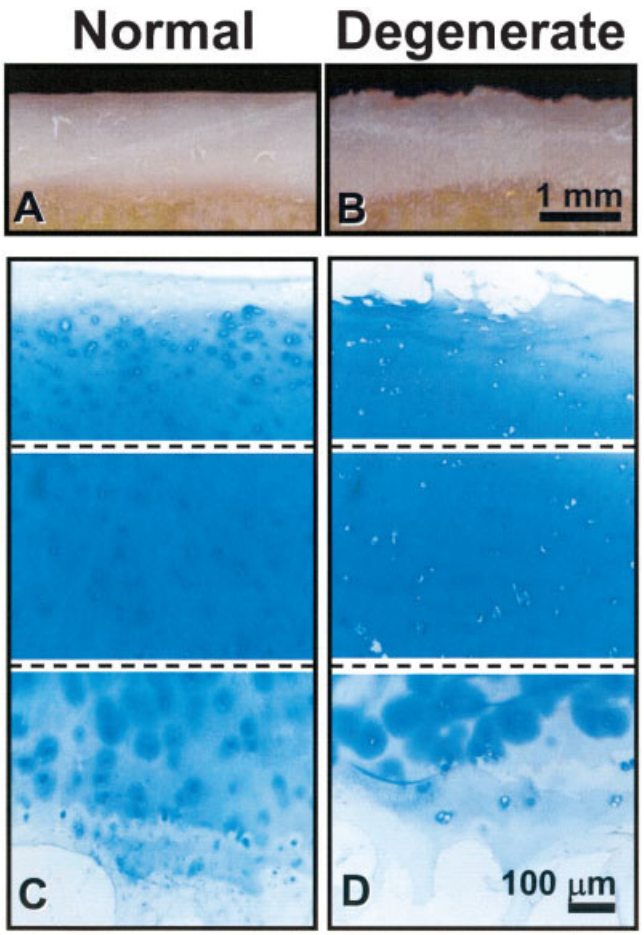

Figure 2. A and **B**, Photographs of cross-sections of samples of normal and degenerated cartilage. **C** and **D,** Representative micrographs of Alcian blue–stained sections, showing structure detail of normal (**C**) and degenerated (**D**) cartilage. Color figure can be viewed in the online issue, which is available at http://www.arthritisrheum.org.

testing, this time with SF (pooled from adult bovine knees and stored at −80°C) plus PI as the lubricant. The SF had been characterized previously for boundary lubrication properties (7) and for levels of lubricant molecules (~1 mg/ml of hyaluronan and 0.45 mg/ml of proteoglycan 4 [21]). The same regions of interest as used in studies with PBS were imaged. Then, samples were allowed to reswell.

Finally, samples were tested in a macroscale shear system to assess overall mechanical properties of cartilage in shear, as described below.

Microscale shear testing. Each sample, consisting of paired osteochondral blocks, was bathed for ~14–18 hours in test lubricant containing PI and propidium iodide (20 μg/ml) at 4°C to fluorescently highlight cell nuclei prior to microscale shear testing. Each pair of osteochondral blocks (Figures 1B and D) was then placed with cartilage in apposition in a custom biaxial loading chamber mounted onto an epifluorescence microscope for digital video imaging (4). The chamber secured one block at the bone and allowed in-plane movement of the apposing mobile block along the x-directed 8-mm lengths of the samples (Figure 1D), with orthogonally positioned plungers interfaced with either a micrometer (for axial displacement) (model 262RL; Starrett, Athol, MA) or motion-controller (for lateral displacement) (model MFN25PP; Newport, Irvine, CA). Fluorescence images (G-2A filter; Nikon, Melville, NY) with a field of view of ~3 × 2 mm^2 were obtained at 5 frames/second, showing a full-thickness region of cartilage in the secured block and a partial-thickness region of cartilage in the apposing block.

Cartilage deformation in the secured block was assessed during axial and shear loading. First, the block was imaged in the reference state (uncompressed). Then, axial displacement (~40 μm/second) was applied by the micrometer to induce 15% compression ($1 - \Lambda_z$, where Λ_z is the stretch ratio [22]) of the cartilage tissue (Figure 1C), during which time sequential images (~1.5% compression increment/frame) were acquired. Samples were then allowed to stress-relax for 1 hour, which was calculated to be sufficient to reach an approximate equilibrium stress based on consideration of the characteristic time constant. Experimentally, this duration of stress-relaxation was validated to be sufficient with load decreasing to 50% of the peak by 130 seconds, and load at 1 hour being only 3 ± 1% (mean ± SEM; n = 3) higher than the load at 16 hours. Subsequently, lateral motion was applied to the mobile osteochondral block (Figure 1D). Two sets of lateral displacements (Δx), each consisting of +1 mm and then −1 mm (returning to initial position), were applied at 100 μm/second to the bone portion of the mobile block. The first set, followed by a pause of 12 seconds, was for preconditioning (7), while the second set was recorded for analysis. The sliding velocity was chosen based on the range of velocities (0–0.1 m/second) occurring during the loading (stance) phase of gait (23,24). Before and during the application of lateral displacements (Figure 1D), sequential images, with ~10 μm of lateral movement of the mobile block between frames, were obtained.

Macroscale shear testing. To assess the overall compressive and shear biomechanical properties of the cartilage of the secured block, following microscale shear tests, each secured block was subjected to a macroscale test using a biaxial mechanical tester (Mach-1 V500CS; BioSyntech, Montreal, Quebec, Canada). Test conditions were chosen to match the mechanical deformation observed in the microscale shear test, but with instrumentation allowing measurement of axial and shear loads. Each sample block was affixed, compressed 15% at a rate of 0.03%/second using a rigid stainless steel platen (~2 μm pore size, providing a no-slip boundary condition), and allowed to stress-relax for 1 hour to reach equilibrium. With increasing lateral displacement, continuous and monotonically increasing shear load waveforms were observed, confirming no-slip conditions; a plateau in shear load, which would indicate slip, was not observed. Equilibrium force was recorded and normalized to the 3 × 8 mm^2 area to yield an estimate of the equilibrium compressive stress. Next, 2 sets of lateral displacements of the amplitude occurring at the surface at the onset of sliding in microscale shear tests were applied at a rate of 100 μm/second, held for 10 seconds while shear load was being recorded, and released. A pause of ~12 seconds followed the first set of lateral displacements, during which the cartilage sample was continuously hydrated in PBS plus PI. As in the microscale tests, the first set was for preconditioning, while the second set was used for analysis. The lateral displacements were then repeated in the reverse direction following a 5-minute pause, and shear loads occurring in the last second of the 10-second load-capture period in both directions were averaged. This average shear load was normalized to the 3 × 8 mm^2 area to yield an estimate of the shear stress (at which sliding occurred in the microscale test).

Data collection and calculations. Digital micrographs were analyzed to determine the depth-varying and overall strains in cartilage. Images were analyzed with MatLab 7.0 (MathWorks, Natick, MA) using software routines similar to those described previously (14,25,26). Briefly, an evenly distributed set of cell nuclei (~250 cells/mm^2), which served as fiducial markers, was selected and tracked by maximizing cross-correlation of regions surrounding each marker with the preceding, and then initial, frames. Generally, chondrocyte nuclei in normal tissue were available, and were chosen in regions up to the true articular surface (defined by a discontinuity in displacement during sliding), while for degenerated tissue, nuclei were visible up to ~50–70 μm (~3%) below the true surface, due to fibrillation. Local affine mappings of nuclei were used to calculate the displacement ($\bar{u}$) of uniformly spaced (10-pixel) mesh points in the region of interest (~1 mm × full thickness) during deformation (Figure 1D). Displacement gradients ($\partial\bar{u}/\partial z$, $\partial\bar{u}/\partial x$) were then determined by finite difference approximations, and in turn, used to determine Lagrangian compressive strain (E_{zz}) after axial compression and shear strain (E_{xz}) after lateral shearing, with these Lagrangian strains being appropriate for finite strains as well as small strains (27).

This method was validated, and interobserver variability was assessed. Using mathematically transformed images, the calculated strain values deviated by less than 0.005 ± 0.005 (mean ± SEM) from the theoretical values, with the error being proportionately smaller in regions exhibiting lower amplitudes of strain. Interobserver variability, assessed as the average of the SD in calculated strain between 3 observers, was ~0.01 for a subset of data from all sample types (n = 4). Here

also, the variability was proportionately lower in regions of relatively small shear magnitudes.

The calculated shear strain was interpolated, averaged depthwise, and plotted as a function of tissue depth, normalized to the cartilage thickness in the compressed state. Shear strain was interpolated linearly at every 5% of the normalized tissue thickness near the articular surface (i.e., 0–0.3) and every 10% for remaining regions of the tissue depth (i.e., 0.3–1) after applied compression and prior to lateral motion. To consolidate data, strain values were averaged at the same normalized depth (0 [surface] and 1 [tidemark]) to yield a depth profile. Shear strain results were determined when surfaces were sliding, at which time shear strain was at a peak and no further changes in deformation occurred with additional lateral displacement (i.e., sliding). The overall Lagrangian shear strain was defined as half the lateral surface displacement normalized to the compressed cartilage thickness. Since the shear strain peaked near the articular surface, shear strain occurring at the top 5% was also compared.

Overall cartilage properties were determined from forces recorded during compression and shear. Under compression alone, the compressive modulus of cartilage was defined as the increment in stress divided by the increment in applied compressive strain. The overall shear modulus (G) for each sample was determined as the increment in shear stress (shear load divided by surface area) divided by the increment in shear strain.

The depth-varying shear moduli were estimated from the overall shear modulus and local shear strain in each sample. Since shear modulus is inversely related to shear strain, and with shear stress assumed to be constant at all depths, the local shear modulus was estimated as the overall shear modulus multiplied by the overall shear strain and divided by the local shear strain. Because these estimates depend on shear strain in the denominator, shear modulus was calculated at every 10% of the tissue depth near the articular surface (up to 20% of the depth) and every 20% of the tissue depth in the subsequent regions, to reduce noise.

Statistical analysis. Data are reported as the mean ± SEM, unless noted otherwise. Repeated-measures analysis of variance was used to determine the effects of normalized tissue depth (0–1 [surface–bone]), lubricant (PBS or SF), and degeneration (normal or degenerated) on tissue shear strain, and to determine the effects of tissue depth and degeneration on shear modulus.

RESULTS

Histopathologic findings. The overall histopathology scores were consistent with the gross (Figures 2A and B) and histologic (Figures 2C and D) appearance of normal and degenerated samples. Degenerated samples had significantly ($P < 0.01$) higher histopathology scores than normal samples (Table 1). In degenerated samples, structural (surface irregularity, vertical clefts to transitional zone, and transverse clefts) and cellular (cloning) features exhibited mild degeneration and were scored ~1-point higher than the corresponding features in normal samples. In contrast, cellularity and GAG staining scores were similarly low (i.e., normal) in normal and degenerated samples. These results confirmed that gross visualization resulted in an appropriate selection of normal and mildly degenerated samples, for articulation testing.

Compressive deformation and properties. The axial compression of cartilage in the secured block resulted in compressive strain that varied significantly with depth from the articular surface ($P < 0.001$) but not between normal and degenerated samples ($P = 0.6$). E_{zz} was relatively high near the articular surface (mean ± SEM 0.38 ± 0.05) and relatively low in the deepest regions (0.06 ± 0.01). Transverse-oriented (E_{xx}) and shear (E_{xz}) strain resulting from the applied compression was low, averaging <0.03 in all samples. The equilibrium compressive modulus (E) in the full-thickness cartilage was not significantly different between sample groups ($P = 0.5$) (mean ± SEM 0.79 ± 0.13 MPa in normal cartilage and 0.61 ± 0.23 MPa in degenerated cartilage).

Shear deformation. Qualitatively, cartilage shear loading resulted in a sequence of 4 events: 1) At the onset of applied lateral displacement, cartilage surfaces initially adhered and began to move laterally in unison. 2) With increasing lateral displacement, lateral deformation and hence E_{xz} increased and occurred throughout the tissue depth. 3) Next, lateral deformation and E_{xz} of cartilage peaked, just as the surfaces detached and slid relative to each other. 4) With additional lateral displacement, the cartilage deformation and E_{xz} were maintained at a steady-state peak.

At the steady state, tissue displacement and E_{xz} (Figure 3) were nonuniform and depth-varying, with shear magnitudes that were high near the articular surface and low (almost indistinguishable) near the bone. The mean ± SEM maximum lateral displacement of apposing surfaces before slipping when lubricated with SF was 115 ± 14 μm and 82 ± 16 μm in normal and degenerated tissue, respectively. When lubricated with PBS, maximum lateral displacement in normal and degenerated tissue was 169 ± 12 μm and 125 ± 18 μm, respectively, before slipping. Differences in shear deformation between normal and degenerated samples were also evident (Figure 3). Shear deformation in degenerated samples (Figures 3C and D) was concentrated near the surface, while in normal samples, deformation occurred further into the tissue depth (Figures 3A and B).

Quantitatively, the E_{xz} of articulating cartilage

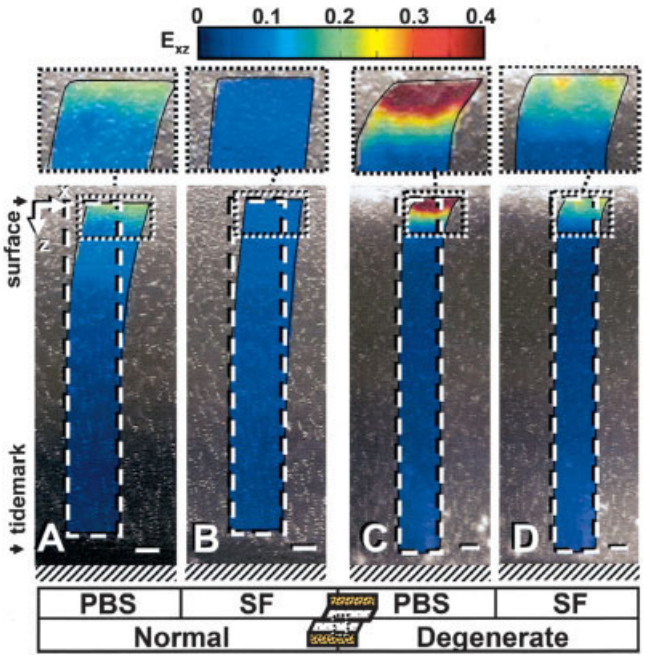

Figure 3. Micrographs obtained during shear loading of apposing normal (**A** and **B**) and degenerated (**C** and **D**) cartilage samples lubricated with phosphate buffered saline (PBS) (**A** and **C**) or synovial fluid (SF) (**B** and **D**), after maximum shear strain was achieved. The cell nuclei tracking method was used to create maps of shear strain (magnified above each panel; boxes with dotted lines indicate magnified areas). Dashed lines surround the analyzed regions on the undeformed images. Schematic at the bottom depicts the sample and testing configuration, with the dotted-line box representing the area from which the images shown were obtained and analyzed. Bars = 100 μm.

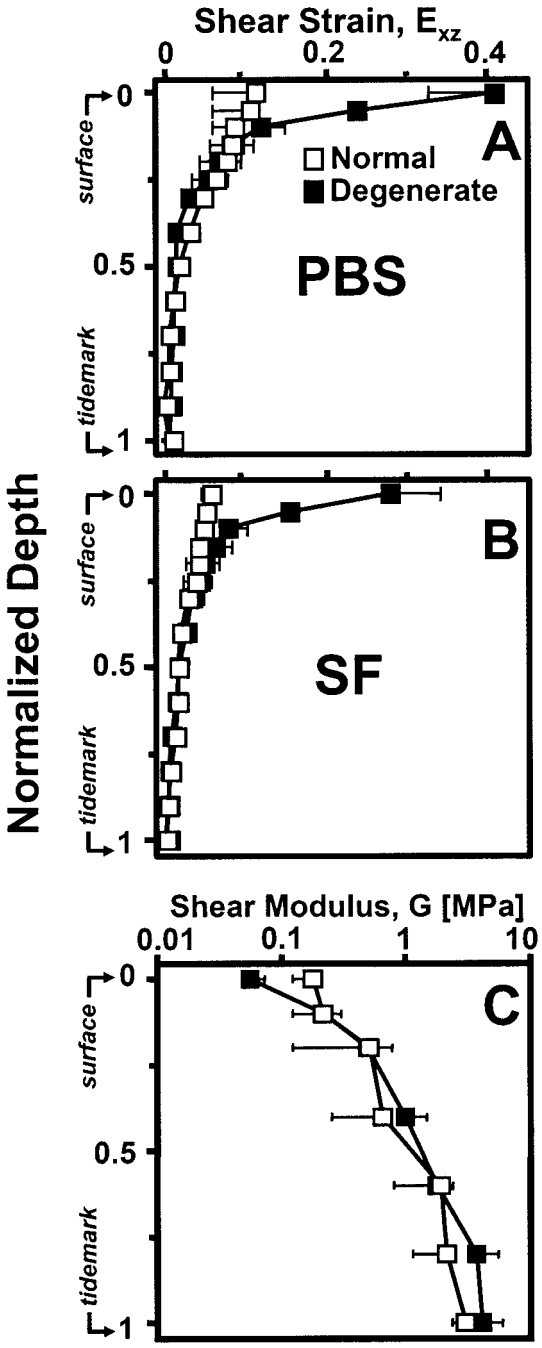

Figure 4. Biomechanical measures of adult human articular cartilage in shear. **A** and **B,** Local shear strain (E_{xz}) versus normalized tissue depth in normal and degenerated cartilage, as determined by microscale shear testing. Samples were tested with phosphate buffered saline (PBS) (**A**) or synovial fluid (SF) (**B**) as lubricant. **C,** Local shear modulus (G) versus normalized tissue depth in normal and degenerated samples, as determined by macroscale testing. Values are the mean and SEM.

varied with depth from the articular surface, lubricant, and surface degeneration. In the depth profile of E_{xz} (Figures 4A and B), the highest values were obtained near the articular surface, and E_{xz} decreased monotonically with depth ($P < 0.001$). The variation of E_{xz} with depth depended on surface degeneration ($P < 0.001$ for the interaction), with E_{xz} decreasing more with depth in the degenerated sample. A similar trend was noted with testing using PBS, where E_{xz} decreased at greater rates with depth than when tested with SF ($P < 0.001$ for the interaction) in both normal and degenerated samples. The combined effect of depth and either degeneration or lubricant on shear strain was evidenced as varying E_{xz} values near the surface, but similarly low values of E_{xz} (<0.01) in the deep layer of cartilage.

Peak E_{xz} at the surface ($z = 0$) (Figure 5A) and overall E_{xz} (Figure 5B) were each significantly affected by both the lubricant used and degeneration status. The peak surface E_{xz} (Figure 5A) was ~3–5 times higher in

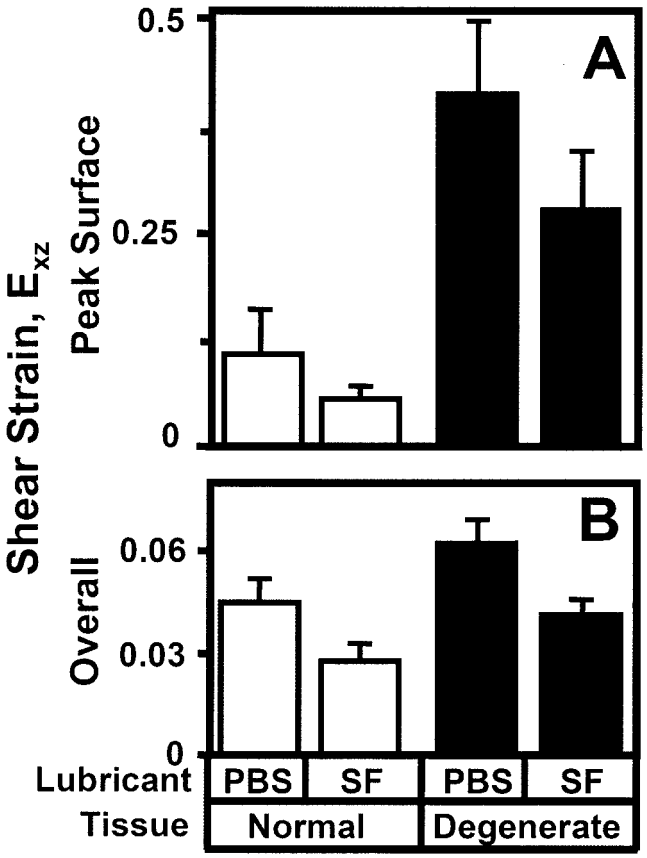

Figure 5. Effect of sample group (normal or degenerated cartilage) and of lubricant (phosphate buffered saline [PBS] or synovial fluid [SF]) on **A,** peak surface shear strain and **B,** overall shear strain. Values are the mean and SEM.

samples with surface degeneration than in normal tissue ($P < 0.05$) with both surface lubricants. With PBS, the mean of the peak surface (Figure 5A) E_{xz} increased from 0.11 (normal samples) to 0.41 (degenerated samples). With SF, E_{xz} increased from 0.056 (normal samples) to 0.28 (degenerated samples). In addition, peak surface E_{xz} values obtained when tested with PBS were ~1.5–2 times the values obtained when tested with SF ($P < 0.05$). Overall E_{xz} (Figure 5B) was not detectably different between normal and degenerated samples ($P = 0.10$) when tested using the same lubricant. However, overall E_{xz} did vary with lubricant. The overall E_{xz} of normal tissue was significantly lower with SF than with PBS (0.028 versus 0.045), and the overall E_{xz} of degenerated tissue was 0.041 with SF versus 0.062 with PBS ($P < 0.05$ for both).

Shear properties. To replicate sample shear deformation in microscale shear tests, lateral surface displacements in macroscale shear tests ranging from 70 to 125 μm (measured from microscale shear tests) were applied to normal samples, and 120–160 μm was applied to degenerated samples. Overall G was not significantly different between normal and mildly degenerated tissue (mean ± SEM 0.32 ± 0.09 MPa in normal and 0.26 ± 0.07 MPa in degenerated cartilage; $P = 0.7$). G was lowest near the articular surface and increased significantly with tissue depth ($P < 0.01$) (0.2–-0.6 times and 10–15 times the overall G near the surface and in the deepest region, respectively) (Figure 4C). At all depths below the surface, G was not significantly different between normal and degenerated samples ($P > 0.5$). Near the articular surface, there was a trend toward lower G values with mild surface degeneration ($P = 0.10$) (surface G = 0.18 ± 0.06 MPa and 0.06 ± 0.02 MPa in normal and degenerated samples, respectively).

DISCUSSION

This study elucidated the shear deformation and strain of cartilage during contact and sliding, as well as the effects of lubrication and mild degeneration, using a microscale cartilage-on-cartilage testing system. The present results indicate that cartilage–cartilage articulation results in 4 sequential events: adherence, adherence and deformation, detachment, and sliding. Peak E_{xz} was highest near the surface and modulated by both the lubricant used and the condition of the sample itself (Figures 4A and B). Relative to the use of normal SF as lubricant, E_{xz} increased with the use of PBS by ~100% near the surface (Figure 5A) and ~55% overall (Figure 5B). In addition, when degenerated samples were tested, their E_{xz} values near the surface were ~3–5 times higher than those of normal samples (Figure 5A).

Osteochondral samples used in this study were prepared from a site that is affected by age-associated degeneration and osteoarthritis. The samples were from the lateral femoral condyle, a load-bearing region where ~22% of arthroscopically diagnosed chondral defects occur (28,29). The biomechanical factors associated with early degeneration in such load-bearing regions may contribute to the progressive degeneration of articular cartilage. Although the samples used had been previously frozen, a single freeze–thaw cycle does not result in marked changes in compressive properties of normal (30) or degenerated (31) articular cartilage or its structure (32), and is thus unlikely to have marked effects on shear properties. Although the distal femoral condyle normally apposes the tibial plateau, cartilage from the femoral condyle was apposed against itself to create a

simplified symmetric loading situation. Cartilage from other sites could be examined in future studies.

The testing protocol used in this study provides a mechanical environment mimicking the compression and sliding of articular cartilage during normal joint loading. A knee undergoes a wide range of dynamic compression (up to 5–20%) (1,2) and sliding (up to ~50 mm) during normal activities (estimated from refs. 23 and 24). The present analysis addresses certain parts of the gait cycle (e.g., contralateral toe-off and heel rise [23]) in which compressive loading is high and sliding velocity is low, during which time interaction of apposing tissue surfaces is likely to be initiated. Since samples were allowed to stress-relax for 1 hour, the pattern of cartilage deformation and strain is likely to be representative of that occurring after prolonged cyclic loading and sliding, rather than that which occurs at the onset of cyclic loading. Cartilage gradually depressurizes and reaches an averaged steady-state compression under prolonged cyclic loading. During this time, interstitial fluid pressure diminishes (33), and boundary lubrication becomes increasingly important (7). The rate-dependence of shear deformation was not assessed; however, shear deformation may not change markedly with rate of lateral displacement since kinetic friction remains fairly constant with sliding velocity (7). Additional studies might elucidate the time course of cartilage shear after the onset of loading, as well as effects of sliding velocity on shear deformation.

Although edge effects may occur in this shear testing protocol, such effects are likely minimal in the central area of tissue that was analyzed. Boundaries of the analyzed region were ~2 mm away from both the leading and the trailing edges of the samples. Recent studies have shown that intratissue deformation (Gratz KR, et al: unpublished observations) and stiffness (34) are affected only ~1–2 mm from vertical boundaries of cartilage. Thus, the results are likely to be representative of the major areas of cartilage contact.

The reduction in E_{xz} with SF as lubricant is consistent with predictions derived from a variety of past studies on cartilage friction. The friction coefficient decreases with the use of SF as lubricant compared with saline, both in cartilage-on-cartilage in the boundary mode (7,35) and in whole joint (36–38) friction tests. Assuming cartilage material properties (i.e., compressive and shear modulus) are maintained with the use of SF and PBS, the friction-reducing property of SF would be predicted to result in a reduction of tissue E_{xz}.

The overall E_{xz} values obtained in this study are consistent with values estimated during physiologic joint articulation based on previously reported material properties of cartilage, as follows. To provide a first-order estimate of tissue properties, cartilage can be modeled as a linear, homogeneous, isotropic, and elastic tissue. With such assumptions and under small strain conditions, the overall stiffness of cartilage in shear (G) can be related to the shear stress (σ_{xz}) and the resulting overall E_{xz} (27) as follows: $G = \sigma_{xz}/2E_{xz}$ (equation 1). In addition, σ_{xz} acting on cartilage can be related to the friction coefficient (μ) and normal contact stress (σ_n) as follows: $\sigma_{xz} = \mu\sigma_n$ (equation 2). Substituting equation 2 into equation 1 and rearranging terms, cartilage E_{xz} can be expressed as $E_{xz} = \mu\sigma_n/G$ (equation 3).

Using reported values of μ (~0.01) (39) and σ_n (~2 Mpa) (40) and the overall G values of ~0.2–0.4 MPa found in this study, the estimated overall E_{xz} is 0.02–0.05. The estimate of E_{xz} is consistent with the range of overall E_{xz} determined in this study (Figure 5B). This suggests that an overall E_{xz} ranging from 0.01 to 0.1 may be suitable for biomimetic in vitro simulation of physiologic shear loading, for example during mechanical evaluation and mechanical stimulation for tissue engineering of cartilage.

The increased E_{xz} with degeneration, particularly near the surface with SF as lubricant (Figure 5A), appears to be due to both increased friction between sliding surfaces and a reduction in tissue shear modulus. Roughened surfaces have local asperities that can cause increased interaction and adherence between tissue surfaces, enhancing friction during sliding. Since boundary lubricants modulate friction, higher E_{xz} in degenerated cartilage when tested in PBS (Figure 5A) indicates that friction between degenerated surfaces is higher than that between normal surfaces. Additionally, with degeneration, cartilage mechanical properties, such as G, become impaired (12). Diminished G would result in increased cartilage E_{xz} at the same magnitude of σ_{xz} (equation 3), even if friction coefficient were similar. Since surface E_{xz} increased with degeneration with the use of SF as lubricant, and G near the surface tended to diminish with degeneration, the elevated E_{xz} at the surface in mildly degenerated tissue is likely a result of both increased μ and reduced G (equation 3 and Figure 5A).

Depth variations in E_{xz} and G in the cartilage samples used in the present study provide additional information on the depth-varying biomechanical properties of articular cartilage. Compressive strain is depth-varying in both statically (4) and dynamically (3) compressed cartilage, decreasing monotonically with depth from the articular surface. E_{xz} observed in this study was similarly depth-varying, being highest near the surface

and lowest near the tidemark (Figures 4A and B). Compressive modulus, deduced from the overall compressive stress and local strain, was reflective of the depth-varying strain magnitudes, with cartilage increasing in stiffness with increasing depth (4). Similarly, G was lowest near the articular surface and increased monotonically to a maximum (20%) in the deepest region (Figure 4C). While G near the surface only tended to decrease with degeneration, the lack of statistical significance was likely due to the calculation from 2 measurements, shear stress and strain (each having variability), as well as donor variability.

The overall unconfined compressive modulus at equilibrium found in this study (E = 0.79 MPa) is consistent with previously reported values in human cartilage (0.58 MPa) (41). The overall shear properties of human cartilage have yet to be reported; however, overall G can be estimated from Poisson's ratio (ν) and the aggregate modulus (H_A) demonstrated in indentation tests, using the relationship

$$G = \frac{H_A(1 + \nu)(1 - 2\nu)}{2(1 + \nu)(1 - \nu)}$$

(27,42). The overall G found in this study (0.32 MPa) is consistent with that estimated from indentation tests (0.2–0.4 MPa) (43). Thus, for cartilage in compression, the deformation and mechanical properties we observed are consistent with findings of previous studies, and for cartilage in shear, the newly described depth-varying strain and shear properties are within values predicted for full-thickness human cartilage.

With cartilage degeneration, tissue structure and low cellularity may affect the analysis and interpretation of deformation and strain. Degenerated cartilage contains clefts and areas of erosion (20), both of which result in material discontinuities within cartilage. Thus, continuum assumptions are not strictly valid. Also, compatibility conditions (27) are not maintained when fibrillated tissues overlap during deformation. Nevertheless, the present samples were only mildly degenerated and relatively intact except at the surface, and, whereas there were few visible cells at the surface of the degenerated samples, cells near the surface (3–5% depth) could be tracked. From a linear extrapolation, this may have resulted in a slight (~15%) underestimation of the absolute magnitude of superficial shear strain.

The present results suggest that changes in E_{xz} magnitudes and shear behavior may contribute to cartilage degeneration and pathogenesis. While samples were tested with a common overall compressive strain in this study, marked differences in E_{xz} between groups occurred even with this conservative testing protocol. Under similar loads instead of overall strain, softer tissues (i.e., degenerated cartilage) would exhibit larger compressive and shear strain, excessive levels of which can contribute to cartilage degeneration. Excessive magnitudes of compressive strain result in mechanical injury to cells (44,45) and matrix (45,46), leading to reduced cartilage remodeling, maintenance, and repair. Likewise, high E_{xz} that results from degenerated matrix, along with deficient lubrication, may lead to additional degeneration. Cell death and matrix damage may spread with continued exposure to high E_{xz}, diminishing local mechanical properties of cartilage in both compression and shear. Cartilage E_{xz} may then further increase and further the changes in tissue structure, resulting in a self-propagating cycle of degeneration. Such mechanical effects may also induce changes in surrounding joint tissues and the biochemical environment, which could supplement cartilage deterioration.

ACKNOWLEDGMENTS

We thank the many residents and staff at Dr. Lotz's Laboratory at the Scripps Research Institute for harvesting and providing the human tissue used in this study, and Barbara Schumacher for guidance on histopathologic processing.

AUTHOR CONTRIBUTIONS

Dr. Sah had full access to all of the data in the study and takes responsibility for the integrity of the data and the accuracy of the data analysis.

Study design. Wong, Bae, Sah.
Acquisition of data. Wong, Chun, Lotz.
Analysis and interpretation of data. Wong, Bae, Gratz, Sah.
Manuscript preparation. Wong, Bae, Sah.
Statistical analysis. Wong, Bae, Sah.

REFERENCES

1. Eckstein F, Lemberger B, Stammberger T, Englmeier KH, Reiser M. Patellar cartilage deformation in vivo after static versus dynamic loading. J Biomech 2000;33:819–25.
2. Kersting UG, Stubendorff JJ, Schmidt MC, Bruggemann GP. Changes in knee cartilage volume and serum COMP concentration after running exercise. Osteoarthritis Cartilage 2005;13: 925–34.
3. Neu CP, Hull ML, Walton JH. Heterogeneous three-dimensional strain fields during unconfined cyclic compression in bovine articular cartilage explants. J Orthop Res 2005;23:1390–8.
4. Schinagl RM, Gurskis D, Chen AC, Sah RL. Depth-dependent confined compression modulus of full-thickness bovine articular cartilage. J Orthop Res 1997;15:499–506.
5. Ateshian GA, Lai WM, Zhu WB, Mow VC. An asymptotic solution for the contact of two biphasic cartilage layers. J Biomech 1994;27:1347–60.
6. Swanson SAV. Friction, wear, and lubrication. In: Freeman MAR,

editor. Adult articular cartilage. 2nd ed. Tunbridge Wells (UK): Pitman Medical; 1979. p. 415–60.
7. Schmidt TA, Sah RL. Effect of synovial fluid on boundary lubrication of articular cartilage. Osteoarthritis Cartilage 2007;15: 35–47.
8. Schmidt TA, Gastelum NS, Nguyen QT, Schumacher BL, Sah RL. Boundary lubrication of articular cartilage: role of synovial fluid constituents. Arthritis Rheum 2007;56:882–91.
9. Elsaid KA, Jay GD, Warman ML, Rhee DK, Chichester CO. Association of articular cartilage degradation and loss of boundary-lubricating ability of synovial fluid following injury and inflammatory arthritis. Arthritis Rheum 2005;52:1746–55.
10. Clark JM, Simonian PT. Scanning electron microscopy of "fibrillated" and "malacic" human articular cartilage: technical considerations. Microsc Res Tech 1997;37:299–313.
11. Meachim G, Emery IH. Quantitative aspects of patello-femoral cartilage fibrillation in Liverpool necropsies. Ann Rheum Dis 1974;33:39–47.
12. Setton LA, Elliott DM, Mow VC. Altered mechanics of cartilage with osteoarthritis: human osteoarthritis and an experimental model of joint degeneration. Osteoarthritis Cartilage 1999;7:2–14.
13. Sah RL, Grodzinsky AJ, Plaas AHK, Sandy JD. Effects of static and dynamic compression on matrix metabolism in cartilage explants. In: Kuettner KE, Schleyerbach R, Peyron JG, Hascall VC, editors. Articular cartilage and osteoarthritis. New York: Raven Press; 1992. p. 373–92.
14. Wang CC, Deng JM, Ateshian GA, Hung CT. An automated approach for direct measurement of two-dimensional strain distributions within articular cartilage under unconfined compression. J Biomech Eng 2002;124:557–67.
15. Chahine NO, Wang CC, Hung CT, Ateshian GA. Anisotropic strain-dependent material properties of bovine articular cartilage in the transitional range from tension to compression. J Biomech 2004;37:1251–61.
16. Yamada K, Healey R, Amiel D, Lotz M, Coutts R. Subchondral bone of the human knee joint in aging and osteoarthritis. Osteoarthritis Cartilage 2002;10:360–9.
17. Scott JE, Dorling J. Differential staining of acid glycosaminoglycans (mucopolysaccharides) by alcian blue in salt solutions. Histochemie 1965;5:221–33.
18. Ross MH, Kaye GI, Pawlina W. Histology: a text and atlas. 4th ed. Philadelphia: Lippincott Williams & Wilkins; 2003.
19. Bae WC, Temple MM, Amiel D, Coutts RD, Niederauer GG, Sah RL. Indentation testing of human cartilage: sensitivity to articular surface degeneration. Arthritis Rheum 2003;48:3382-94.
20. Shapiro F, Glimcher MJ. Induction of osteoarthrosis in the rabbit knee joint: histologic changes following menisectomy and meniscal lesions. Clin Orthop Rel Res 1980;147:287–95.
21. Mazzucco D, Scott R, Spector M. Composition of joint fluid in patients undergoing total knee replacement and revision arthroplasty: correlation with flow properties. Biomaterials 2004;25: 4433–45.
22. Fung YC. Biomechanics: mechanical properties of living tissues. 2nd ed. New York: Springer-Verlag; 1993.
23. Whittle M. Gait analysis: an introduction. 3rd ed. Oxford (UK): Butterworth-Heinemann; 2002.
24. Shelburne KB, Torry MR, Pandy MG. Muscle, ligament, and joint-contact forces at the knee during walking. Med Sci Sports Exerc 2005;37:1948–56.
25. Bae WC, Lewis CW, Levenston ME, Sah RL. Indentation testing of human articular cartilage: effects of probe tip geometry and indentation depth on intra-tissue strain. J Biomech 2006;39: 1039–47.
26. Gratz KR, Sah RL. Experimental measurement and quantification of frictional contact between biological surfaces experiencing large deformation and slip. J Biomech 2008;41:1333–40.
27. Fung YC. A first course in continuum mechanics. 2nd ed. Englewood Cliffs (NJ): Prentice-Hall; 1977.
28. Hjelle K, Solheim E, Strand T, Muri R, Brittberg M. Articular cartilage defects in 1,000 knee arthroscopies. Arthroscopy 2002; 18:730–4.
29. Curl WW, Krome J, Gordon ES, Rushing J, Smith BP, Poehling GG. Cartilage injuries: a review of 31,516 knee arthroscopies. Arthroscopy 1997;13:456–60.
30. Swann AC, Seedhom BB. The stiffness of normal articular cartilage and the predominant acting stress levels: implications for the aetiology of osteoarthrosis. Br J Rheumatol 1993;32:16–25.
31. Kempson GE, Spivey CJ, Swanson SA, Freeman MA. Patterns of cartilage stiffness on normal and degenerate human femoral heads. J Biomech 1971;4:597–609.
32. Kiefer GN, Sundby K, McAllister D, Shrive NG, Frank CB, Lam T, et al. The effect of cryopreservation on the biomechanical behavior of bovine articular cartilage. J Orthop Res 1989;7: 494–501.
33. Armstrong CG, Lai WM, Mow VC. An analysis of the unconfined compression of articular cartilage. J Biomech Eng 1984;106: 165–73.
34. Bae WC, Law AW, Amiel D, Sah RL. Sensitivity of indentation testing to step-off edges and interface integrity in cartilage repair. Ann Biomed Eng 2004;32:360–9.
35. Forster H, Fisher J. The influence of loading time and lubricant on the friction of articular cartilage. Proc Inst Mech Eng [H] 1996; 210:109–19.
36. Wright V, Dowson D. Lubrication and cartilage. J Anat 1976;121: 107–18.
37. Linn FC. Lubrication of animal joints. II. The mechanism. J Biomech 1968;1:193–205.
38. Mabuchi K, Tsukamoto Y, Obara T, Yamaguchi T. The effect of additive hyaluronic acid on animal joints with experimentally reduced lubricating ability. J Biomed Mater Res 1994;28:865–70.
39. Tanaka E, Kawai N, Tanaka M, Todoh M, van Eijden T, Hanaoka K, et al. The frictional coefficient of the temporomandibular joint and its dependency on the magnitude and duration of joint loading. J Dent Res 2004;83:404–7.
40. Raimondi MT, Pietrabissa R. Contact pressures at grafted cartilage lesions in the knee. Knee Surg Sports Traumatol Arthrosc 2005;13:444–50.
41. Jurvelin JS, Buschmann MD, Hunziker EB. Mechanical anisotropy of the human knee articular cartilage in compression. Proc Inst Mech Eng [H] 2003;217:215–9.
42. Mow VC, Hayes WC, editors. Basic orthopaedic biomechanics. 2nd ed. New York: Raven Press; 1997.
43. Athanasiou KA, Rosenwasser MP, Buckwlter JA, Malinin TI, Mow VC. Interspecies comparisons of in situ intrinsic mechanical properties of distal femoral cartilage. J Orthop Res 1991;9:330–40.
44. Loening A, Levenston M, James I, Nuttal M, Hung H, Gowen M, et al. Injurious mechanical compression of bovine articular cartilage induces chondrocyte apoptosis. Arch Biochem Biophys 2000; 381:205–12.
45. Chen CT, Bhargava M, Lin PM, Torzilli PA. Time, stress, and location dependent chondrocyte death and collagen damage in cyclically loaded articular cartilage. J Orthop Res 2003;21:888–98.
46. Thibault M, Poole AR, Buschmann MD. Cyclic compression of cartilage/bone explants in vitro leads to physical weakening, mechanical breakdown of collagen and release of matrix fragments. J Orthop Res 2002;20:1265–73.